Chinese Chemical Letters 31 (2020) 2849–2853

Contents lists available at ScienceDirect

Chinese Chemical Letters

journal homepage: www.elsevier.com/locate/cclet

Communication

Highly efficient enrichment and adsorption of rare earth ions (yttrium(III)) by recyclable magnetic nitrogen functionalized mesoporous expanded perlite

Juan Liu[a,b], Liqiang Zeng[a], Su Liao[a], Xiaofeng Liao[a], Jun Liu[a], Jinshui Mao[a], Yunnen Chen[a], Tingsheng Qiu[a], Sili Ren[a,*]

[a] Jiangxi Key Laboratory of Mining Engineering, School of Resources and Environmental Engineering, Jiangxi University of Science and Technology, Ganzhou 341000, China
[b] School of Chemical Engineering and Materials, Changzhou Institute of Technology, Changzhou 213000, China

ARTICLE INFO

Article history:
Received 21 May 2020
Received in revised form 7 August 2020
Accepted 13 August 2020
Available online 15 August 2020

Keywords:
Rare earth ions
Yttrium(III) ions
Magnetic mesoporous expanded perlite
Enrichment
Adsorption

ABSTRACT

A magnetic mesoporous expanded perlite-based ($EP_{d\text{-}APTES}@Fe_3O_4$) composite was designed and synthesized as a novel adsorbent for enrichment of rare earth ions in aqueous solution. Effect of various factors including the pH of solution, contact time and adsorbent dosage on the adsorption behaviors of yttrium(III) by the $EP_{d\text{-}APTES}@Fe_3O_4$ nano-material composites from aqueous solution was investigated. The maximum adsorption capacity of the as-prepared materials for yttrium(III) ions was 383.2 mg/g. Among the various isotherm models, the Freundlich isotherm model could well described for the adsorption of the rare earth ions at pH 5.5 and 298.15 K. The kinetic analysis indicated that the adsorption process followed the *pseudo*-second order kinetics model, and the rate-determining step might be chemical adsorption. Thermodynamic parameters declared that the adsorption process was endothermic. In addition, Fourier transform infrared spectroscopy (FTIR), X-ray photoelectron spectroscopy (XPS) and the quantum chemical calculation indicated that the yttrium(III) ions were captured on the $EP_{d\text{-}APTES}@Fe_3O_4$ surface mainly by coordination with functional group of $-NH_2$. More importantly, the adsorption-desorption studies indicated that the $EP_{d\text{-}APTES}@Fe_3O_4$ nano-material composites had a high stability and good recyclability.

Rare earth elements (REEs), especially the heavy REEs, play irreplaceable roles in a wide range of advanced technological fields, such as high strength permanent magnets, superconductive material, chemical sensors, luminescent, lasers, hydrogen storage, fiber optics, computer hard disks, cell phones and cameras, due to their special diverse chemical, metallurgical, optical, electronic and catalytic properties [1–4]. The designation of "rare earth" refers to the 17 elements of "lanthanides" series in periodic table, which can be further divided into two groups according to the function of their atomic number. One is "cerium group" (light REE: La, Ce, Pr, Nd, Pm, Sm, Eu, Gd), and the other one is "yttrium group" (heavy REE: Y, Tb, Dy, Ho, Er, Tm, Yb, Lu) [5,6]. Since the beginning of this century, the global consumption of REEs has increased significantly [6]. However, the global reserves of REEs are no more than 99 million tons which limits the use of REEs [7]. Among all REE-based deposits, Bayan Obo deposit is the largest REE-containing deposit but it has high-grade carbonate and low-grade in heavy REEs. While the ion-adsorption type clay deposits in South China, in spite of small in scale and low in grade, dominate the heavy REEs market because of the low mining and processing costs and the high enrichment characteristics of heavy REEs in deposit [8]. To date, the traditional surface mining pool leach process and the *in-situ* leaching mining method are mainly employed to collect the heavy REEs in ion-adsorption type clay. Although most of the REEs in the ion adsorption clay could be collected by these two methods, they do harm to the surrounding environment and waste a substantial part of REEs [9]. It was reported that high concentration of rare earth ions (1-200 mg/L) were found both in downstream of the river and the wastewater of mining and refining factory [10]. Therefore, hundreds of tons of REEs will be lost every year if the wastewater is discharged directly without effective recovery. In addition, the content of REEs in the soil of rare earth mining area is much higher than that in other areas, which leads to the content of REEs in crops, fruits and

* Corresponding author.
E-mail address: sili_ren@163.com (S. Ren).

https://doi.org/10.1016/j.cclet.2020.08.017

vegetables in the mining area exceeding the standard, and accumulating in the body through the food chain, and endangering the health by inhibiting the growth of pre-osteoblasts and poisoning the nervous system [11]. Due to the lack of economic, environmental protection and effective comprehensive recovery methods of low concentration rare earths, the discharge of rare earth wastewater not only causes mass of loss of rare earth resources, but also endangers human health [12]. Therefore, recovering and recycling the REEs in wastewater is thereby an urgent task that needs to be paid much attention.

Up to now, several methods and techniques, such as co-precipitation, filtration, solvent extraction, ion-exchange, liquid membrane and adsorption, have been used for purify, recovery, separation, pre-concentration and enrichment of REEs [2,9,13]. Among these methods, the adsorption by adsorbents including zeolite [14], clay [15], active carbon [16], bioresource materials [5,17], functionalized nano-composites [18–22] has received wide attention because of their simple fabrication process, high efficiency, reusability, low-cost and no secondary pollution. However, the maximum adsorption capacity of the most adsorbents is less than ~200 mg/g [12]. Only a few adsorbents, such as granular grafted hydrogel composites, prawn carapace, sporopollenin/xylan-modified biohydrogel, neem sawdust and granular grafted hydrogel composites, can deliver the adsorption capacity of more than 200 mg/g [2]. Although remarkable progress has been made, the development of high-performance adsorbents with capacity of 350–400 mg/g is still a huge challenge, and the preparation of recyclable high-performance adsorbents is even harder.

Perlite is a glass mineral found in volcanic [23]. When the perlite ore is treated at 750–1700 °C, it expands 10–20 times of its original volume. After the physical transformation, it becomes granular materials with honey comb structure inside [24]. Expended Perlite (EP) has many special properties including high porosity, light weight, high chemical and thermal stability, and exhibits abundance of silanol groups on the porous surfaces. The porous feature and abundant silanol groups on the surface of EP enable it to be easily functionalized through chemical grafting [25], which makes it a promising recyclable adsorbent for recovering the heavy REEs from mining and metallurgy wastewater [26–35].

In this study, magnetic mesoporous expanded perlite was successfully synthesized by grafting the magnetic Fe_3O_4 nanoparticles on amino-group functionalized EP. The precise synthesis procedure and advanced structure endow $EP_{d\text{-}APTES}@Fe_3O_4$ high specific surface area, large number of functionalized sites to effectively adsorb/enrich the heavy REE ions from the wastewater. The synthesis processes of magnetic mesoporous expanded perlite were illustrated in Scheme 1. The detail of synthesis processes, adsorption, characterization, recycle performance and quantum chemical calculations are given in Supporting information.

The $EP_{d\text{-}APTES}@Fe_3O_4$ composite was synthesized *via* a surface grafting strategy followed by a hydrothermal reaction with APTES-decorated EP (noted as $EP_{d\text{-}APTES}$) and $FeCl_3$ as raw material. Fig. 1a show the FTIR of pristine EP powder and 3-aminopropyltriethoxysilane (APTES) molecules decorated EP material. The adsorption bands at ~3458 cm^{-1} is attributed to the combination of −OH stretching of hydrogen-bonded and free Si−OH [23]. The peak at ~1627 cm^{-1} is due to the deformation band of molecular water, while the absorption peaks at ~1100 cm^{-1} and ~790 cm^{-1} are assigned to the Si-O stretching vibrations of Si-O-Si and Si-O-Al, respectively. For the FTIR spectrum of $EP_{d\text{-}APTES}$ powder, the weak peak at 3251 cm^{-1} was assigned to the stretching vibration of -NH_2 groups, indicating the successful decoration of APTES molecules on the surface of EP particles. Besides, the strong peak at 3500 cm^{-1} (Si−OH) shifts to 3650 cm^{-1} due to the disappearance of hydrogen bond. The FTIR of the $EP_{d\text{-}APTES}@Fe_3O_4$ is characterized by a broad peak at 3700–2200 cm^{-1}, and a new peak at 569 cm^{-1}. The broad peak at 3700–2200 cm^{-1} was attributed to the condensation of poly (ethylene glycol), ethylene glycol and sodium citrate to form new functional groups such as double bonds, triple bonds and cumulated diene. These newly formed unsaturated bonds may play a key role in subsequent adsorption of yttrium(III) ions. The new sharp peak at 619 cm^{-1} is attributed to the vibration of Fe-O band [24]. To further validate structure of $EP_{d\text{-}APTES}@Fe_3O_4$, we performed the X-ray diffraction (XRD) measurement on various materials from each stage of preparation. As shown in Fig. 1b, the broad peak of EP and/or APTES-decorated EP at 2θ of 10°-38° that corresponding to amorphous silica, several well-defined diffraction peaks at 2θ of 30.34°, 35.76°, 43.3°, 53.5°, 57.45° and 62.88° are also clearly observed, which can be indexed as (220), (311), (400), (422), (511) and (440) plane reflections of Fe_3O_4, respectively (JCPDS No. 19-0629) [36]. Zeta potential of various materials from each stage of preparation were determined as a function of pH in 1 mmol/L KCl aqueous solutions. As shown in Fig. 1c, the EP particles were negative charged with the average zeta potential value of -13.36 mV with pH 2, while it became positive of 30.73 mV for amino-functionalized $EP_{d\text{-}APTES}$, which was attributed to the protonation of amino groups (-NH_3^+) on the surface. After grafting the Fe_3O_4 particles, $EP_{d\text{-}APTES}@Fe_3O_4$ became less positive than $EP_{d\text{-}APTES}$ due to the formation of Fe_3O_4. As the solution pH is over about 4, the zeta potentials for all the particles became negative. The zeta potential evolution of different materials further confirmed the successful synthesis strategy.

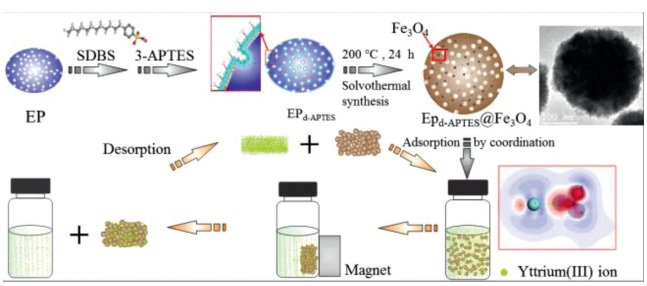

Scheme 1. Schematic illustration of the preparation of $EP_{d\text{-}APTES}@Fe_3O_4$ composites, yttrium(III) adsorption and recycling of the $EP_{d\text{-}APTES}@Fe_3O_4$ adsorbent.

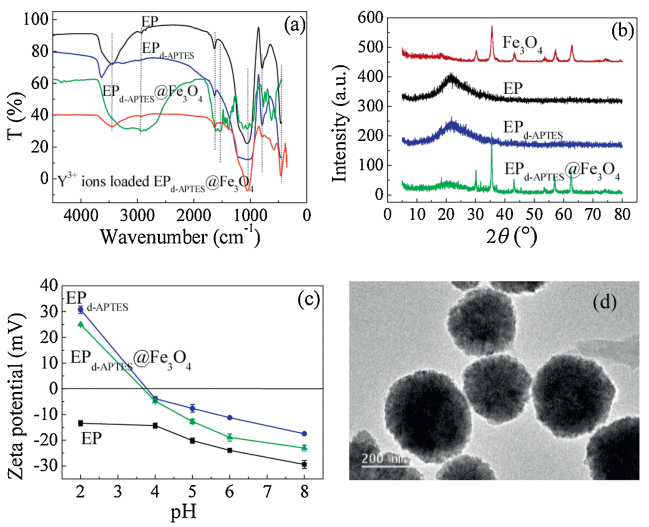

Fig. 1. (a) FTIR spectra of EP, $EP_{d\text{-}APTES}$, $EP_{d\text{-}APTES}@Fe_3O_4$ and yttrium(III) ions loaded $EP_{d\text{-}APTES}@Fe_3O_4$. (b) The XRD patterns of Fe_3O_4, EP, $EP_{d\text{-}APTES}$, and $EP_{d\text{-}APTES}@Fe_3O_4$. (c) Zeta potential of EP, $EP_{d\text{-}APTES}$ and $EP_{d\text{-}APTES}@Fe_3O_4$ as a function of pH in 1 mmol/L KCl. (d) TEM images of $EP_{d\text{-}APTES}@Fe_3O_4$.

The morphology and structure of the various synthesized particles were observed by transmission electron microscope (TEM). The pristine EP are in irregular shaped particles with size of 200−500 nm (Fig. S1a in Supporting information). After being modified by APTES molecules, the resultant $EP_{d\text{-}APTES}$ still remains its irregular shape with almost same size, which is attributed to that the attached monolayer of APTES on the EP surface is very thin (Fig. S1b in Supporting information). After grafting the Fe_3O_4 particles, the shape of the prepared $EP_{d\text{-}APTES}@Fe_3O_4$ composites are changed from the irregular into nearly sphere with size increasing up to 150−400 nm (Fig. 1d). The changes of the size and shape is closely related to the growth of Fe_3O_4 species on the surface of the $EP_{d\text{-}APTES}$ particles. High-magnification TEM image further indicates that the Fe_3O_4 are uniformly grown on the surface of $EP_{d\text{-}APTES}$ particles, forming a typical $EP_{d\text{-}APTES}@Fe_3O_4$ core-shell structure with $EP_{d\text{-}APTES}$ particles as core and nanofiber shaped Fe_3O_4 as shell layer. The growth of Fe_3O_4 on $EP_{d\text{-}APTES}$ surface is associated with the strong hydrogen bond between the -NH_2 group in APTES molecules and hydroxy group in $Fe(OH)_3$ colloids formed during the hydrothermal reaction. The compact deposition of Fe_3O_4 nanofiber on $EP_{d\text{-}APTES}$ particles results in large amounts of voids and interconnected mesoporous structure and thus increase the surface area of $EP_{d\text{-}APTES}@Fe_3O_4$, which will be analyzed by N_2 adsorption/desorption isotherms (Fig. S2 and Table S1 in Supporting information). Other characterizations such as X-ray photoelectron spectrum (XPS) measurement and thermogravimetric analysis (TGA) are illustrated in supporting information (Figs. S3 and 4 in Supporting information). By combining the characterizations, it can be concluded that the Fe_3O_4 has been coated on APTES-modified EP materials and core-shell structured $EP_{d\text{-}APTES}@Fe_3O_4$ was successfully synthesized.

The adsorption behavior and mechanism of $EP_{d\text{-}APTES}@Fe_3O_4$ for yttrium(III) ions were systematically investigated. It is believed that the acidity of the aqueous solution has profound influence on the adsorption behavior because it can affect the state and surface-active sites of the materials. The adsorption behavior of yttrium(III) ions (100 mg/L) on $EP_{d\text{-}APTES}@Fe_3O_4$ was firstly studied under different pH conditions. As shown in the Fig. 2a, the adsorption capacity of $EP_{d\text{-}APTES}@Fe_3O_4$ for yttrium(III) ions increased from 39.40 mg/g to 383.2 mg/g when the pH values was raised from 2 to 5.5. Obviously, the adsorption capacity is relatively low in strong acidic environment, which might be related to the increased surface positive charge because of the protonation of the surface functional groups. For example, the -NH_2 groups lost their coordination ability with yttrium(III) ions due to protonation (-NH_3^+) [37]. Such an inference was supported by the zeta potential characterization of the $EP_{d\text{-}APTES}@Fe_3O_4$ as a function of pH in Fig. 1c, in which the zeta potential was positive with the pH less than ~3.7. The electrostatic repulsion would be occurred or increased between yttrium(III) and the positive charged groups ($Si-OH_2^+$ and -NH_3^+) on the surface of $EP_{d\text{-}APTES}@Fe_3O_4$ [27,34]. In addition, the H^+ ions would also compete with yttrium(III) ions on adsorption in strong acidic environment [38–40]. With the increase of pH value, the zeta potential would also become negative as the solution pH over ~3.7 (Fig. 1c), and the electrostatic attraction would be dominant between $EP_{d\text{-}APTES}@Fe_3O_4$ and yttrium(III) ions. As a result, the adsorption capacity of $EP_{d\text{-}APTES}@Fe_3O_4$ significantly increased. However, as the pH value exceeded ~6.0, the ions started to form insoluble precipitation of hydroxide. Therefore, pH 5.5 was selected to be the optimum pH value for the rest of studies.

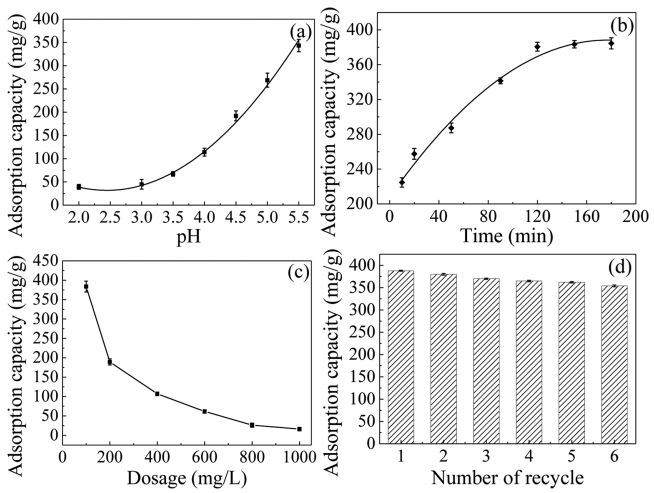

Fig. 2. Effect of solution pH (a), contact time (b) and adsorbent dosage (c) on adsorption capacity of $EP_{d\text{-}APTES}@Fe_3O_4$ for yttrium(III). (d) The recyclability of the $EP_{d\text{-}APTES}@Fe_3O_4$ as adsorbent to adsorb yttrium(III).

For a comparison, the Fe_3O_4 nanoparticles, EP and $EP_{d\text{-}APTES}$ were also used as adsorbents to enrich the yttrium(III) ions (Fig. S5a in Supporting information). It was found that the maximum adsorption capacity of yttrium(III) on Fe_3O_4 nanoparticles, EP and $EP_{d\text{-}APTES}$ were 22.80, 30.25 and 85.32 mg/g, respectively, which were all greatly lower than that of 383.2 mg/g for the $EP_{d\text{-}APTES}@Fe_3O_4$ composites, indicating that the adsorption performance could be greatly improved by the functionalization and Fe_3O_4 nanoparticles grafting of the EP particles.

The effect of contact time on adsorption efficiency of $EP_{d\text{-}APTES}@Fe_3O_4$ for yttrium(III) ions was studied by using 10 mL of the adsorbate solution (100 mg/L) and 1 mg of $EP_{d\text{-}APTES}@Fe_3O_4$ adsorbent. As shown in Fig. 2b, it was observed that the adsorption capacity of $EP_{d\text{-}APTES}@Fe_3O_4$ for yttrium(III) has reached as high as 222.4 mg/g at contact time of 10 min, and then further increased up to 370.5 mg/g at contact time of 120 min, almost approaching the maximum adsorption capacity. Therefore, the optimum contact time in this work was set as 120 min.

Adsorbent dosage is an important factor to affect the adsorption efficiency of the adsorbate. In this study, effect of the adsorbent dosage on adsorption capacity of $EP_{d\text{-}APTES}@Fe_3O_4$ for Yttrium(III) was also investigated. As shown in Fig. 2c, when the dosage was increased from 100 mg/L to 1000 mg/L, its adsorption capacity was correspondingly decreased from 371.6 mg/g to 16.10 mg/g. The decrease of adsorption capacity with increase of dosage is due to the insufficient use of the active sites. Therefore, the optimum dosage was set as 100 mg/L for the rest of adsorption experiments. By combing Figs. 2a-c, it can be concluded that the synthesized $EP_{d\text{-}APTES}@Fe_3O_4$ possesses excellent adsorption performance with maximum adsorption capacity of 383.2 mg/g for rare earth ions of yttrium(III), which is much higher than those in previous reports [41]. The excellent adsorption performance of $EP_{d\text{-}APTES}@Fe_3O_4$ was attributed to the high specific surface area and the large amount of adsorption active sites of amine groups.

The good magnetic property of the $EP_{d\text{-}APTES}@Fe_3O_4$ enables it to be well recycled under the external magnetic field (Fig. 5Sb in Supporting information). As shown in Fig. 2d, for the first adsorption cycle, the adsorption capacity was 388.2 mg/g. Encouragingly, after being recovered and eluted in $(NH_4)_2SO_4$ solution, it still has a good adsorption performance with a high capacity of 354.4 mg/g after six cycles (91.23% of initial adsorption capacity). The findings demonstrate that the $EP_{d\text{-}APTES}@Fe_3O_4$ adsorbent possesses good recyclability and is a promising material for enrichment of the yttrium(III) ions from rare earth wastewater.

To study the adsorption thermodynamics of yttrium(III) ions on $EP_{d\text{-}APTES}@Fe_3O_4$. Three isotherms of langmuir [42], Freundlich [43] and Dubinin-Radushkevic model (D–R isotherm model) [28,44], are used to study the adsorption behavior (Fig. 6S in Supporting

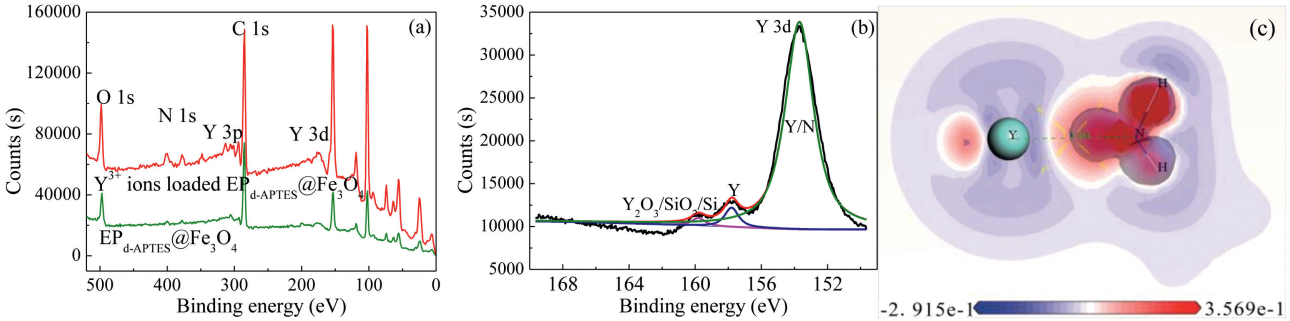

Fig. 3. (a) XPS spectra of $EP_{d\text{-}APTES}@Fe_3O_4$ before and after adsorption of yttrium(III) ions. (b) High-resolution XPS spectra of Y 3d after adsorption of yttrium (III) ions. (c)The electron density differences on the cross section parallel to the surface formed by three atoms (N/Y) for the most stable configuration of yttrium(III) ions interacting with amino group.

information). The result indicated that Freundlich isotherm model could better describe the adsorption process (R^2 = 0.9953). Caculated from D-R isotherm model, the average adsorption energy was 24.1 kJ/mol, indicating that the adsorption is mainly through a chemical adsorption. The adsorption kinetics were also studied in this work [45]. The fitting results show that the *pseudo*-second-order kinetics is suitable for the adsorption of yttrium(III) on the surface of $EP_{d\text{-}APTES}@Fe_3O_4$ (R^2 = 0.9934). In order to investigate the effect of temperature on the adsorption, the thermodynamic parameters were also calculated. The enthalpy change (ΔH^0) had a value of 15.68 KJ/mol at 298.15 K. The positive ΔH^0 indicates that the adsorption is endothermic reaction. The Gibbs free energy change (ΔG^0) of adsorption was calculated to be 5.81 KJ/mol. Therefore, the increase in temperature is beneficial to the adsorption of rare earth ions on $EP_{d\text{-}APTES}@Fe_3O_4$ surface.

To understand the adsorption mechanism of yttrium(III) ions on the $EP_{d\text{-}APTES}@Fe_3O_4$ surface, the FTIR spectrum, XPS measurement and the electron density difference (EDD) were analyzed after $EP_{d\text{-}APTES}@Fe_3O_4$ adsorbing the Yttrium(III) ions. As shown in Fig. 1a, the FTIR spectrum for the yttrium(III) ions loaded $EP_{d\text{-}APTES}@Fe_3O_4$ exhibited a new characteristic weak band at ~460 cm^{-1}, which was attributed to the vibration of Y—N coordination bond. In addition, the broad peak at 3500–2800 cm^{-1} becomes narrower, and the peaks at 565 cm^{-1} and 1532 cm^{-1} disappeared, which further supports the coordination of nitrogen atoms with the yttrium(III) ions [46]. Moreover, the intensity of bands at 3437 cm^{-1} and 2927 cm^{-1} decreased, which might be associated with the coordination of yttrium(III) ions changing the environment of -NH_2 groups. Meanwhile, the XPS spectroscopy is a useful tool to understand the surface chemical states. Fig. 3a shows the XPS spectra of $EP_{d\text{-}APTES}@Fe_3O_4$ before (Fig. S2 in Supporting information) and after adsorption of yttrium(III) ions. For the yttrium(III) ions loaded $EP_{d\text{-}APTES}@Fe_3O_4$ sample, it is obviously observed that two characteristic peaks appear at 299–301 eV and 150–160 eV correspondingly assigned to Y 3p and Y 3d. The high-resolution spectrum of Y 3d is shown in Fig. 3b, which can be fitted to three peaks. Peak at 159.8 eV was assigned to Y_2O_3, which might be resulted from the oxidation of the adsorbed yttrium(III) ions during the drying process of materials after adsorption. The peak at 157.7 eV was attributed to the free yttrium(III) ions adsorbed by a physical process. As to the main peak at 153.7 eV, it was assigned to the yttrium(III) ions coordinated with the functional groups such as -NH_2. Compared with that of the free yttrium(III) ions, the coordination of yttrium(III) ions with -NH_2 groups induces a 4 eV shift toward lower binding energy, which was due to the electron donor effect by the lone electron pair of nitrogen atom. To confirm such a conclusion, the EDD between yttrium(III) ions and amino groups was calculated by using quantum chemical theory.

As illustrated in Fig. 3c, the EDD map reveals the origination of the electronic structure differences upon the bond between the yttrium(III) ion and amino group. The enhanced red religions indicate the electron enrichment, while the enhanced blue regions represent electron deficiency. It can be clearly observed that the electron density of yttrium(III) ion is significantly increased as indicated by the enhanced red color, suggesting that the yttrium(III) ion gains more electrons from amino group. Therefore, it can be concluded that the strong adsorption of yttrium(III) ion on the surface of the synthesized $EP_{d\text{-}APTES}@Fe_3O_4$ composite is closely associated with the coordination of yttrium(III) ions with various functional groups [47].

We have successfully synthesized a magnetic $EP_{d\text{-}APTES}@Fe_3O_4$ composite by amino-functionalizing the EP nanoparticles followed by a Fe_3O_4-decoration process. The synthesized magnetic composite shows a good adsorption behavior for rare earth ions with a high adsorption capacity of 383.2 mg/g for yttrium(III) ions. The adsorption energy from Dubinin-Radushkevic isotherm was estimated to be 24.1 kJ/mol at 298.15 K, indicating that the adsorption of the yttrium(III) on $EP_{d\text{-}APTES}@Fe_3O_4$ is mainly through a chemical adsorption. Adsorption isotherm analysis indicated that the Freundlich isotherm model could better describe the adsorption process of yttrium(III) on $EP_{d\text{-}APTES}@Fe_3O_4$ surface, while the adsorption kinetics complies with the *pseudo*-second-order model. The excellent adsorption properties of the $EP_{d\text{-}APTES}@Fe_3O_4$ materials for yttrium(III) ions are attributed to the porous structure of the materials with high specific surface area on the one hand, and a large number of functional groups of -NH_2 on the surface of the materials on the other hand. The yttrium(III) ions have strong coordination with various functional groups, which were confirmed by FTIR, XPS characterizations and the quantum chemical calculation. More importantly, the synthesized $EPd_{\text{-}APTES}@Fe_3O_4$ composite materials could be recycled for at least six times without significant degeneration in adsorption capacity, indicating that the prepared composites have a high stability and recyclability, and might find its application in treatment of the ionic rare earth wastewater.

Declaration of competing interest

We declare that we have no financial and personal relationships with other people or organizations that can inappropriately influence our work, there is no professional or other personal interest of any nature or kind in any product, service and/or company that could be construed as influencing the position presented in, or the review of, the manuscript entitled “Highly Efficient Enrichment and Adsorption of Rare Earth Ions (Yttrium(III)) by Recyclable Magnetic Nitrogen Functionalized Mesoporous Expanded Perlite”.

Acknowledgments

We acknowledge the financial support by the National Natural Science Foundation of China (No. 51704042), National Key Research and Development Program (No. 2018YFC1903401), Project of Jiangxi Provincial Department of Science and Technology (No. 20202BABL204018), Project of Education Commission of Jiangxi Province of China (No. GJJ170488), Ganzhou Innovative Talents Plane, Natural Science Foundation ofJiangxi University of Science and Technology (No. jxxjbs17042) and National College Students' Innovation and Entrepreneurship Training Program (Nos. 201810407001, 201810407003).

Appendix A. Supplementary data

Supplementary material related to this article can be found, in the online version, at doi:https://doi.org/10.1016/j.cclet.2020.08.017.

References

[1] Y. Hu, S. Giret, R. Meinusch, et al., J. Mater. Chem. A 7 (2019) 289–302.
[2] I. Anastopoulos, A. Bhatnagar, E.C. Lima, J. Mol. Liq. 221 (2016) 954–962.
[3] X. Huang, J. Dong, L. Wang, et al., Green Chem. 19 (2017) 1345–1352.
[4] M. Jha, A. Kumari, R. Panda, et al., Hydrometallurgy 165 (2016) 2–26.
[5] N. Das, D. Das, J. Rare Earth. 31 (2013) 933–943.
[6] P. Emsbo, P.M. cLaughlin, G.N. Breit, et al., Gondwana Res. 27 (2015) 776–785.
[7] Z. Chen, J. Rare Earth. 29 (2011) 1–6.
[8] Y. Kanazawa, M. Kamitani, J. Alloy. Compd. 408-412 (2006) 1339–1343.
[9] T. Dutta, K. Kim, M. Uchimiya, et al., Environ. Res. 150 (2016) 182–190.
[10] X. Du, T. Graedel, Environ. Sci. Technol. 45 (2011) 4096–4101.
[11] V. Gonzalez, D. Vignati, M. Pons, et al., Environ. Pollut. 199 (2015) 139–147.
[12] T. Kegl, A. Kosak, A. Lobnik, et al., J. Hazard. Mater. 386 (2020) 121632.
[13] F. Zhao, E. Repo, Y. Meng, et al., J. Colloid Interf. Sci. 465 (2016) 215–224.
[14] D. Baybaş, U. Ulusoy, J. Hazard. Mater. 187 (2011) 241–249.
[15] G. Moldoveanu, V. Papangelakis, Hydrometallurgy 131-132 (2013) 158–166.
[16] Y. Smith, D. Bhattacharyya, T. Willhard, M. Misra, Chem. Eng. J. 296 (2016) 102–111.
[17] W. Bonificio, D. Clarke, Environ. Sci. Technol. Lett. 3 (2016) 180–184.
[18] J. Florek, F. Chalifour, F. Bilodeau, D. Lariviere, F. Kleitz, Adv. Funct. Mater. 24 (2014) 2668–2676.
[19] J. Roosen, J. Spooren, K. Binnemans, J. Mater. Chem. A 2 (2014) 19415–19426.
[20] T. Ogata, H. Narita, M. Tanaka, Hydrometallurgy 152 (2015) 178–182.
[21] X. Li, T. Lu, Y. Wang, Y. Yang, Chin. Chem. Lett. 30 (2019) 2318–2322.
[22] S. Wu, X. Dai, J. Kan, F. Shilong, M. Zhu, Chin. Chem. Lett. 28 (2017) 625–632.
[23] K. Sodeyama, Y. Sakka, Y. Kamino, H. Seki, J. Mater. Sci. 34 (1999) 2461–2468.
[24] H. Xu, W. Jia, S. Ren, J. Wang, Chem. Eng. J. 337 (2018) 10–18.
[25] L. Maxim, R. Niebo, E. McConnell, Inhal. Toxicol. 26 (2014) 259–270.
[26] M. Dogan, M. Alkan, A. Turkyilmaz, Y. Ozdemir, J. Hazard. Mater. 109 (2004) 141–148.
[27] M. Alkan, M. Karadas, M. Dogan, O. Demirbas, J. Colloid Inter. Sci. 291 (2005) 309–318.
[28] A. Sarı, M. Tuzen, D. Cıtak, M. Soylak, J. Hazard. Mater. 148 (2007) 387–394.
[29] Z. Talip, M. Eral, Ü. Hiçsönmez, J. Environ, Radioact. 100 (2009) 139–143.
[30] H. Ghassabzadeh, M. Torab-Mostaedi, A. Mohaddespour, et al., Desalination 261 (2010) 73–79.
[31] H. Ghassabzadeh, A. Mohadespour, M. Torab-Mostaedi, et al., J. Hazard. Mater. 177 (2010) 950–955.
[32] T. Dong Nguyen, M. Singh, P. Ulbrich, N. Strnadova, F. Stepanek, Sep. Purif. Technol. 82 (2011) 93–101.
[33] D. Nguyen Thanh, M. Singh, P. Ulbrich, et al., Sep. Purif. Technol. 82 (2011) 93–101.
[34] S.M. Turp, Desalin. Water Treat. 142 (2019) 205–212.
[35] W. Long, X. Tan, B. Xiao, N. Han, F. Xing, J. Clean. Prod. 213 (2019) 406–414.
[36] H. Deng, X. Li, Q. Peng, et al., Angew. Chem. Int. Ed. 44 (2005) 2782–2785.
[37] T. Yang, C. Shen, Z. Li, et al., J. Phys. Chem. B 109 (2005) 23233–23236.
[38] C. Huang, Rare Earth Coordination Chemistry, 1st ed., Wiley, Singapore, 2010.
[39] E. Repo, J. Warchol, A. Bhatnagar, M. Sillanpaa, J Colloid Inter. Sci. 358 (2011) 261–267.
[40] S. Banerjee, D. Chen, J. Hazard. Mater. 147 (2007) 792–799.
[41] M. Xu, P. Hadi, G. Chen, G. McKay, J. Hazard. Mater. 273 (2014) 118–123.
[42] D. Martin, L. Jalaff, M. Garcia, M. Faccini, Nanomaterials 9 (2019) 1648.
[43] G. Zaimes, B. Hubler, S. Wang, V. Khanna, ACS Sustain. Chem. Eng. 3 (2015) 237–244.
[44] Y. Liu, M. Chen, Y. Hao, Chem. Eng. J. 218 (2013) 46–54.
[45] S. Lagergren, Vetenskapsakad. Handl. 24 (1898) 1–39.
[46] A. Aziz, M.A. Sayed, Anal. Biochem. 598 (2020) 113645.
[47] J.R. Gispert, Coordination Chemistry, 1st ed., Wiley, Weinheim, 2008.